Investigation of and mechanism proposal for solvothermal reaction between sodium and 1-(2-hydroxyethyl)piperidine as the first step towards nitrogen-doped graphenic foam synthesis

Lilian Moumaneix, Jenifer Guerrero Parra, Sébastien Fontana, François Lapicque, Claire Herold

Investigation and mechanism proposal of solvothermal reaction between sodium and 1-(2-Hydroxyethyl)Piperidine as the first step towards nitrogen-doped graphenic foam synthesis

Received 00th January 20xx,
Accepted 00th January 20xx

DOI: 10.1039/x0xx00000x

Lilian Moumaneix,[a] Jenifer Guerrero Parra,[a] Sébastien Fontana,[a] François Lapicque,[b] and Claire Hérold *[a]

In view to synthetizing 3-dimensional nitrogen-doped graphenic materials, which could be used as oxygen reduction catalyst in membrane fuel cells, a solvothermal-based route has been successfully carried out. However, the solvothermal reaction between metallic sodium and 1-(2-hydroxyethyl)piperidine (HEP), the latter being the source of both carbon and nitrogen, is still little understood. The present work was aimed at investigating the solvothermal process, under different conditions of temperature, pressure and different amounts of sodium. Use of in-situ mass spectroscopy during the three-day reaction revealed the early formation of dihydrogen, as well as carbon oxides, methane and ammonia, in addition to fragment of ethylpiperidine alkoxide (EP-ONa). XRD measurements evidenced the formation of sodium-based compounds, e.g. hydride, carbonate, hydroxide, cyanide. Interestingly, Raman spectroscopy revealed the significant presence of large aromatic molecules as well as a sp^2 carbon network, early precursor of graphene. Analysis of the overpressures and reaction yields led to suggest that the primary compound of HEP reaction with sodium is a large sp^2 carbon-based network entrapping numerous sodium-based molecules as well as a volatile liquid phase. The suggested reactional mechanism provides information to better tailor the solvothermal products, whose pyrolysis at 850 °C lead to very high specific area nitrogen-doped carbon materials.

A Introduction

Supercritical fluids (SCF) provide distinctive experimental media as their properties strongly depend on both internal pressure and temperature. Halfway between gas and liquids states, supercritical fluids give great opportunities to have control over many physical properties, e.g. reactivity, density, polarity or viscosity [1]. SCF possess liquid-like densities (0.2-0.9 $g.cm^{-3}$), gas-like viscosities (1-9 x 10^{-5} $Pa.s^{-1}$) and intermediary diffusivities (2-7 x 10^{-8} $m^2.s^{-1}$) [2].

Technologies based on SCF are daily used in many industrial applications such as the extraction of numerous organic molecules from agricultural products e.g. aroma from plants, caffeine from coffee, cold sterilization, impregnation at heart or plastic packaging treatment. In materials science, phenomena made possible by SCF media can be of a great interest for synthesis or post-treatment methods for numerous materials.

With regard to carbon materials, literature contains several examples of SCF applications to process nanocarbon materials including graphenic materials. Nowadays, graphene is widely studied in numerous scientific fields thanks to its electric, thermal, chemical and mechanical properties. Numerous operations can be achieved on carbon materials in SCF conditions e.g. graphite exfoliation [3,4], synthesis of graphene composites [5], elaboration of three-dimensional graphenic materials [6–8] or deposition of metal nanoparticles on graphene materials [9].

In the last decades, various research works had focused on obtaining three-dimensional graphenic materials such as crumpled graphene sheets, graphene frameworks or graphene foams through a solvothermal-based process. A solvothermal reaction is defined as a reaction in a closed system between reagents in the presence of a solvent (which can be part of the reagents) at a temperature higher than the boiling point of the solvent. If both pressure and temperature are above those of the solvent critical point (below respectively), the solvothermal reaction is said in supercritical conditions (subcritical conditions respectively). In addition to allowing reaction occurrence at moderate temperatures, closed system processes also help with the reduction in noxious emissions in environment [10]. A heat treatment is often needed after the reaction to convert the carbon-rich solvothermal product to well-organized graphenic materials. This route of synthesis allows to recover substantial quantity of graphenic material and possesses a good potential for scalability towards industrial processes [10]. In 2004, Kuang et al. [11] reported the elaboration of crumpled graphene nanosheets by the reaction between tetrachloromethane (CCl_4) and potassium in an autoclave heated at 60 °C for 10 hours. Eftekhari et al. [12] adapted this synthesis route to produce curly graphene sheets by adding cobalt chloride which acts as a catalyst to transform graphene sheets into carbon nanotubes. In parallel, several works dealt with oxidation reactions of sodium in contact with an alcohol, e.g. methanol, ethanol or butan-1-ol [13–17]. In their study, Choucair et al. [13] synthesized crumpled graphene sheets using ethanol and sodium. The solvothermal reaction was carried out at 220 °C for 72 h, followed by a flash pyrolysis. They proposed a mechanism based on the encapsulation of free-ethanol by saturated metal alkoxide in a clathrate-like structure during the solvothermal reaction to explain the obtained structure. However, complementary investigations would be required to confirm their original theory. Speyer et al. [14–16] considered nearly the

[a] Institut Jean Lamour, CNRS – Université de Lorraine, 2 allée André Guinier, 54011 Nancy, France.
[b] Laboratoire Réactions et Génie des procédés, CNRS – Université de Lorraine, ENSIC, 54000 Nancy, France.
† Corresponding author: Dr. Claire Herold claire.herold@univ-lorraine.fr
+33372742537

same process but applied 100 bar upon nitrogen introduction into the reactor to increase furthermore the pressure during the reaction. Graphenic samples showed a noticeable improvement in their crystallinity. These publications and other works not cited here, display the possibility to transform small organic molecules into large sp^2 3-dimensional graphenic networks, using a convenient, highly adaptable technique.

Recently, nitrogen-doped carbon materials have attracted great attention due to their potentials as critical metal-free catalysts [18–20], their semi-conducting properties or their capacity to provide good anchors for metal nanoparticles nucleation [21, 22]. Synthesized by arc-discharge-based synthesis [23], chemical vapor deposition (CVD) [24], thermal treatment [25, 26], plasma treatment [27] or metallothermic reduction [28] high quality N-doped carbon materials can also be prepared through a direct solvothermal-based synthesis [29–32]. However, only a few examples of solvothermal synthesis of N-doped graphenic materials have been reported so far. Tetrachloromethane (CCl_4) is a common precursor used when mixed with lithium nitride (Li_3N) [29], Li_3N and cyanuric chloride $(NCCl)_3$ [30] or with pyrrole (C_4H_5N) and potassium [31]. However, the formation of chlorine-derived gases could be avoided by changing the reagents and the reaction conditions. In a previous study [33], a solvothermal-based process using a mixture of cyclohexanol, ethanolamine and sodium, was developed for the synthesis of good quality nitrogen-doped graphenic foam, whose extensive characterization revealed high surface area, good crystallinity and promising catalytic properties. Moreover, this study allowed determination of the optimal temperature of pyrolysis at 850 °C, yielding N-doped graphenic foams with the best compromise between homogeneity, purity and crystallinity, along with appreciable synthesis yields.

The present paper has focused on the solvothermal reaction, which has been very little investigated by itself up to now. For this pioneering work, it was preferred to consider the reaction of a single molecule being the sources of C and N atoms: 1-(2-hydroxyethyl)piperidine ($C_7H_{15}NO$), subsequently called HEP, and metallic sodium, here combined in view to form, after a subsequent pyrolysis treatment, high-quality nitrogen-doped graphenic foams. The variation of the solvothermal product with the reaction parameters has been followed using complementary techniques for better understanding the reactional mechanism involved here and more generally for carbon materials synthesis through solvothermal-based processes.

B Materials and methods

B.1. Synthesis

A mixture of 0.17 mol of 1-(2-hydroxyethyl)piperidine (ACROS organics, 99%) was put in contact with a certain amount of metallic sodium (Merck Millipore) under inert atmosphere (nitrogen Air Liquide, Alphagaz 2) in a 0.5 L Parr autoclave. 1-(2-hydroxyethyl)piperidine was used as received. Sodium rods were washed in petroleum ether to remove the paraffin oil, then scraped before use to remove the passivation layer formed even under protective atmosphere. Theoretical critical conditions of 1-(2-hydroxyethyl)piperidine have been estimated around 385 ± 29 °C and 37 ± 7 bar using computational models [34–36]. Thus, the solvothermal reaction has been carried out at 300 °C, 350 °C and 380 °C, further increase in temperature being avoided for technological reasons. The solvothermal reaction pressure has been varied between 100 bar and 200 bar, a range which have been proved in previous works suitable for synthesis of high-quality graphenic materials [33]. Once the autoclave sealed, nitrogen (Air Liquide, Alphagaz 2) was introduced so that the internal pressure at the reaction temperature could reach its desired level at 100 bar or 200 bar. The reactor was then heated up at 8 °C.min^{-1} to the targeted temperature and the internal pressure reached the desired value. The mixture was let to react for 72 h, then allowed to cool down to room temperature. The internal pressure inside the autoclave was measured and the solvothermal product was recovered and stored under nitrogen atmosphere. Because solvothermal products are poorly stable in air, characterizations were thus carried out as fast as possible, keeping the product within inert atmosphere as long as possible.

B.2. Characterizations

Raman spectroscopy investigations were conducted with a Renishaw inVia Quontor equipped with a 532 nm laser operating in the spectral range 100-3600 cm^{-1} in synchroscan mode. HEP was simply poured inside a watch glass, the laser beam being focused just under the surface of the liquid. Solvothermal products were kept inside sealed silica quartz cells to avoid any contact with air.

X-Ray diffraction (XRD) were performed on a Bruker D8 Advance diffractometer using Mo(Kα1) radiation, λ = 0.70930 Å. Analysed samples were introduced in 1.5 mm wide Lindemann glass capillaries under nitrogen (nitrogen Air Liquide, Alphagaz 2) atmosphere.

In situ mass spectrometry was carried out using a solvothermal reactor directly connected to a mass spectrometer Pfeiffer Vacuum Prisma. The pressure in the entire device was controlled at the desired level using a set of valves. Measured intensities were normalized to the N_2 peak (channel 28) in order to perform proper comparisons throughout the analysis without influence from slight changes in the measured gas flow.

Table 1: Sample identifications, reaction parameters and experimental results

Sample ID	Na/HEP ratio	Reaction temperature T (°C)	Pressure at T (bar)	Overpressure at room temperature (bar)	Reaction yield (wt. %)	Aspect
SP-T/300	1,5	300	207	4	61	Very oily
SP-T/350	1,4	350	208	15	69	Oily
SP-T/380	1,5	380	207	12	66	Dry
SP-R/1.0	1	350	203	14	62	Very oily
SP-R/1.5	1,4	350	208	15	69	Oily
SP-R/2.0	2	350	204	11	60	Dry
SP-P/100	1,5	380	100	18	61	Dry
SP-P/200	1,5	380	207	12	66	Dry

Molecular masses in the range 0-120 g.mol^{-1} were investigated, no peaks being identifiable above this limit. Compounds identification was achieved using the National Institutes of Standards and Technology (NIST) library as a reference.

C Results and discussion

C.1. Pressure and reaction yield investigations

Regarding the stoichiometry generally considered for the reaction between sodium and an alcohol (equation 1), the reaction yield and released pressure can be calculated. EP stands for 1-ethylpiperidine.

$$HEP + Na \rightarrow EP\text{-}ONa + \tfrac{1}{2}H_2 \qquad \text{Equation 1}$$

Because sodium is always introduced in the same or higher quantity than HEP, the latter one will be considered as being limiting in equation 1. Considering a total reaction, the final molar amount of EP-ONa is then equal to the initial molar HEP amount. The amount of H_2 produced is equal to half the one of HEP initially introduced, i.e. 0.087 mol here. The reaction yield was defined as the ratio between the amount of solvothermal product recovered over the maximum amount of EP-ONa that could be obtained, taking into account the excess of sodium introduced.

The theoretical pressure released by the formation of H_2 has been estimated using the ideal gas law. Considering the volume of the solvothermal reactor, the theoretical partial pressure of hydrogen at room temperature (293 K) was calculated as 4.24 bar (4.24 x 10^5 Pa). The overpressures displayed in table 1 and figure 1 result from the difference between the pressure of N2 injected at room temperature before the heating, and the final pressure, measured at room temperature, after the reaction.

In this study, the impact of three parameters has been investigated, namely solvothermal reaction temperature and pressure as well as the molar ratio between sodium and HEP. Table 1 gathers the operating conditions considered and elements on the products obtained. The uncertainty on the pressure measures was estimated at ± 1 bar. As full recovery of the solvothermal product from the reactor can be troublesome because of its high viscosity, the loss in solvothermal product was estimated to be lower than 1 g, leading to an uncertainty in the reaction yield near ± 5 wt.%. Please note that runs SP-T/350 and SP-R/1.5 as well as SP-T/380 and SP-P/200 are strictly identical but have been given different names for the sake of clarity.

The reaction yields and overpressures are reported in figure 1. Theoretical H_2 partial pressure as expected from equation 1 has been added to evidence the difference in pressure between theory and experiments.

The obtained results are interesting in many aspects. Firstly, the overpressure before opening the solvothermal reactor at ambient temperature, was found in all cases larger than the theoretical hydrogen overpressure, expressing the fact that the postulated reaction given in equation 1 would not be the only chemical process: other reactions leading to the formation of gas species would then occur.

Secondly, the overpressure value can be correlated to that of reaction operating conditions. An increase in the solvothermal reaction temperature causes an elevation of the overpressure, from 4 ± 1 bar to 12 ± 1 bar at 300 °C and 380 °C respectively, with a slight decrease between 350 °C and 380 °C (cf. figure 1 (a)). This increase in pressure could be due to the promoting of gas creating reactions at higher temperatures compared to the lowest one. On the contrary, an increase in the Na/HEP ratio at constant temperature results in a reduction in the overpressure, from 14 ± 1 bar to 11 ± 1 bar for a Na/HEP ratio of 1.0 and 2.0 respectively (cf. figure 1 (b)). Addition of sodium

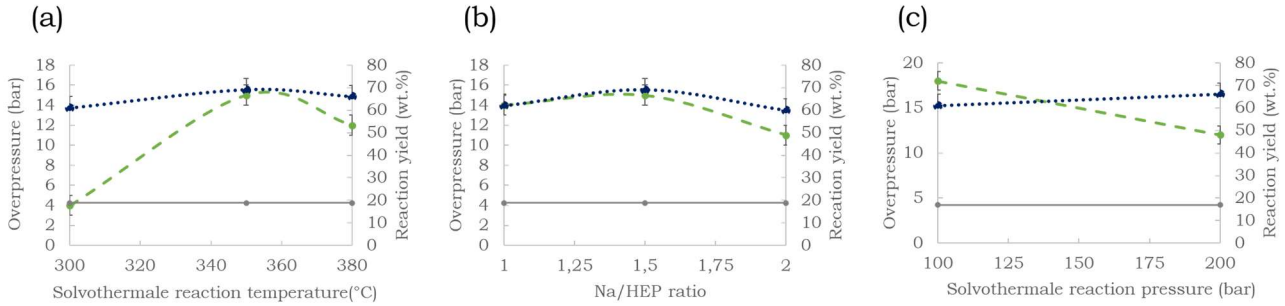

Figure 1: Theoretical gas overpressure (grey line), experimental gas overpressure (green dashed line) and yield (dark blue dotted line) with the evolution of the solvothermal reaction temperature (a), Na/HEP ratio (b) and solvothermal reaction pressure (c)and/or hinder the reactions leading to the formation of gaseous

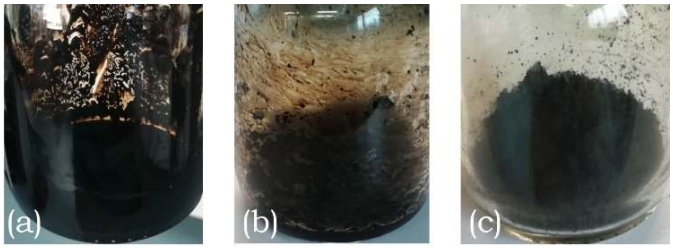

Figure 2: Photographs of solvothermal products presenting a very oily aspect (a), oily aspect (b) and dry aspect (c)

could reduce the overpressure by reacting with the gas phase species. A decrease in overpressure is also observed with a larger solvothermal reaction pressure, from 18 ± 1 bar to 12 ± 1 bar at 100 bar and 200 bar respectively (cf. figure 1 (c)). The less observed mass loss. Formation of heavier molecules could also be imagined, such as oxidation products CO, NO, CO_2 or NO_2. In this case, a relationship between the overpressure and the mass loss could be established. However, the initial amount of oxygen atoms inside the reactor is insufficient to produce such amounts of carbon or nitrogen oxides. Formation of volatile organic compounds could moreover be envisaged but it is unlikely that their volatility would correspond to overpressure at room temperature over 10 bar.

Regarding the obtained results and calculations, the direct correlation between the gas and solid phases does not suffice to fully explain the losses of mass in the solid phase. After cooling down and measurement of the gas pressure, solvothermal products were recovered and calculations of reaction yields were achieved however, only after opening of the reactor and subsequent release of part of the gas phase: a loss of matter due to the sudden decompression is likely to happen and may explain the yields usually below 70 wt.%. This phenomenon will be further discussed later in this paper.

Solvothermal products can also be visually characterized by their physical aspects and more especially their oily aspect. As this introduced parameter is difficult to quantify, also because of their instability in air, a qualitative appreciation has been given using three different denominations. The first one is “very oily” and has been applied for samples presenting a liquid phase, often presenting a brownish colour. The second one is “oily” and has been given to samples containing a unique solid phase but susceptible to leave oily traces on the glass flask. The last one is “dry” and correspond to powdery samples leaving no oily trace in their flasks. Photographs illustrating these denominations are presented in figure 2.

The aspect of solvothermal product is given in table 1, along with the reaction conditions. Solvothermal products pass from very oily to oily and then dry by increasing the temperature or the Na/HEP ratio.

At 300 °C, liquid compounds are present in high quantities in comparison to the solids formed. By increasing the temperature to 350 °C, this liquid phase appears partly replaced by a solid phase, being in little significant amount upon further increase to 380 °C. This phenomenon could be either explained with thermal decomposition or thermally favoured conversion reactions. A slight change of colour, from brown to perfectly black, has also been observed with the increase in temperature, indicating that the solvothermal product obtained at 380 °C is likely carbon-richer than the one obtained at 300 °C, more especially with a larger density of conjugated double bonds.

Similar observations have been made upon increase in Na/HEP ratio, from 1.0 to 2.0, except for the colour remaining dark brownish for the powdery sample SP-R/2.0. The less marked oily aspect can be attributed to the higher number of possible reactions with Na, which is present in greater excess as the Na/HEP ratio increases. Thus, the liquid phase is more likely to react with the available sodium to give solid sodium compounds such as NaOH or Na_2CO_3. No visible change has been observed with the increase in solvothermal reaction pressure, this parameter being possibly less critical in the range investigated than solvothermal reaction temperature or Na/HEP ratio. Pressures above 100 bar do not seem to be determinant to form dry compounds. However, experiments not presented here showed that a 100-bar pressure leads, after a pyrolysis step, to poor quality N-doped graphenic foams.

C.2. Gas phase characterization: Mass spectrometry investigations

In situ mass spectrometry has been used to investigate the gas phase throughout a typical solvothermal reaction, carried out at 380°C and 200 bar with a Na/HEP ratio of 1.5. These conditions have been chosen as they are known to produce the graphenic material with the highest quality after thermal post-treatment (data not shown here). Channels of interest have been plotted over reaction time in figure 3. The log scale in the plots has been used only because of the large range in order of magnitude of the signal. The in-situ analysis was preceded by a blank test, without reagents introduced in the reactor, which allowed to take into account the impurities in the glove bag atmosphere, such as traces of O_2, CO_2 and H_2O. Values from the blank analysis have been added in the form of orange dotted lines in figure 3 (a-e).

Analysis of collected data shows a fast change in the gaseous phase composition within the first hours of the reaction. A large increase in the intensity of channel 2 (cf. figure 3 (a)), related to H_2, coupled with the appearance of peaks at m/z = 98, 99, 84 and 85 (cf. figure 3 (f)), associated with solvothermal alkoxide EP-ONa fragments, demonstrate the occurrence of the reaction between Na and HEP (equation 1). Moreover, since the

significant gas phase formation can simply be explained by Le Chatelier’s principle and has been previously reported in literature as a compression effect [37], being mostly favourable to the creation of denser structures.

Finally, the reaction yields always ranged from 60 wt.% to 70 wt.%. However, in a sealed reactor every loss of matter must result in the formation of another product, being in solid, liquid or gaseous state. Different hypotheses have been expressed and tested to explain the observed loss of matter. A direct relation between the overpressure and the low yields has been firstly considered. This overpressure could be due to the release of light molecules, e.g. H_2, CH_4, H_2O, coming from the degradation of the solvothermal product. However, the low molar masses of such molecules do not suffice to explain the

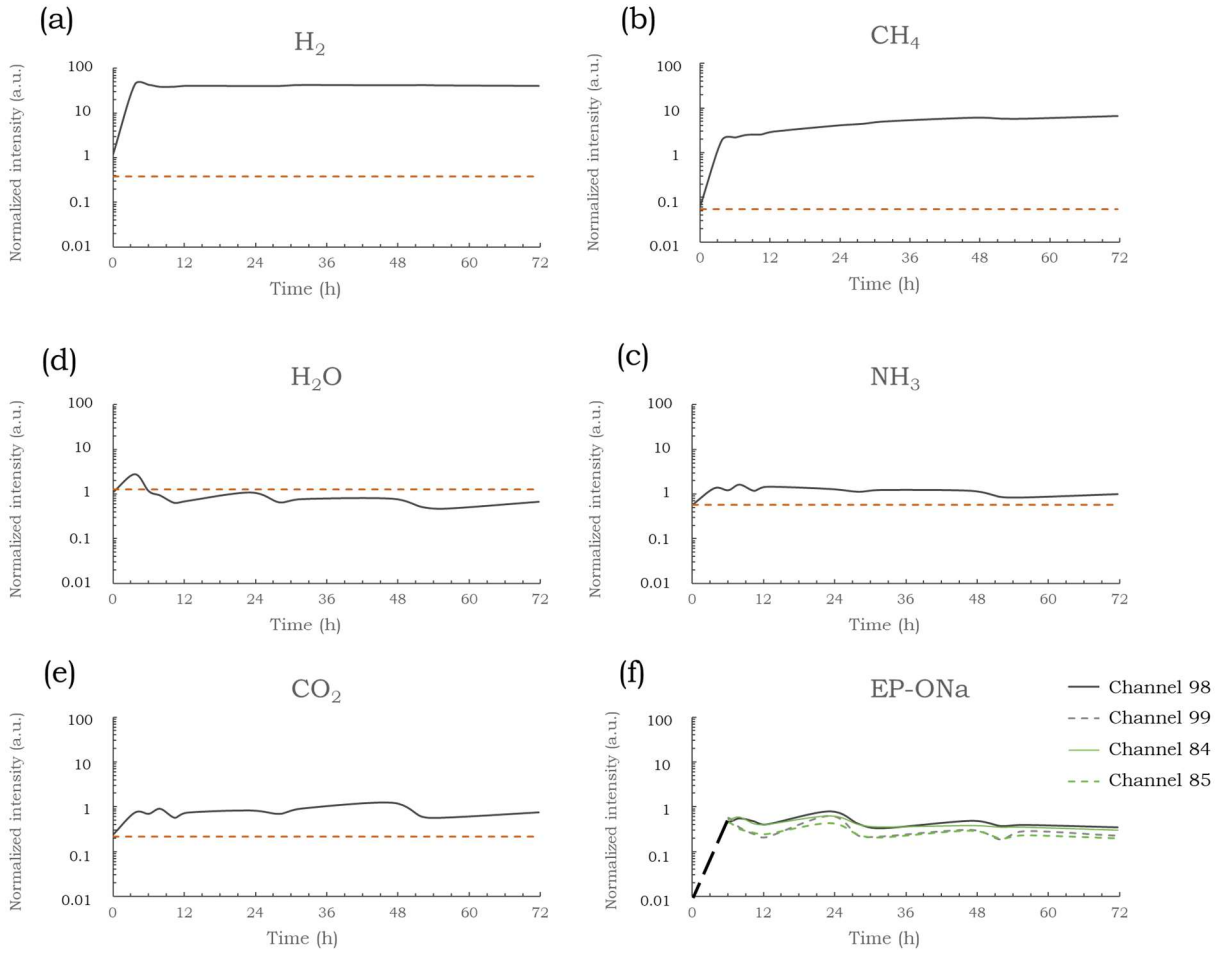

Figure 3 : Time variation of channel signals associated with H2 (a), CH4 (b), NH3 (c), H2O (d), CO2 (e) and solvothermal alkoxide EP-ONa(f); the orange dotted lines are the signal for the blank test; the black dashed line has been added on the EP-ONa graph to better visualize the apparition of this product; solvothermal conditions: 380 °C, 200 bar, Na/HEP 2.0

intensities of both H_2 and EP-ONa channels tend to stabilize after a few hours, it is likely that this reaction be completed within this time lapse or reach a steady level.

Signal intensity of channels 15, 17 and 44 (cf. figure 3 (b, c, e)) related to CH_4, NH_3 and CO_2 respectively, increased rapidly in the first hours of the synthesis. This shows the occurrence of secondary reactions, which are likely responsible for the increase in the final gas pressure discussed in the previous part. CH_4 intensity increased around 40-fold in the first hours, then followed by a steady but far slower increase with time: the intensity was three times higher at the end of the run (4300 min) than at 220 min. The steady rise in CH_4 could be related to the thermal degradation of the solid phase, rich in carbon atoms, throughout the synthesis. Additionally, methanation reactions are highly suspected to occur, as high pressures and the temperature domain investigated are known to favour CO and CO_2 conversion to CH_4 [38]. Methane formation usually occurs through a set of four main gas-phase reactions, involving reverse water-gas shift (equation 2), CO methanation (equation 3), reverse dry reforming (equation 4) and CO_2 methanation (equation 5) [39]. Formation of CO could not be followed since its molecular weight (m/z = 28) is the same as that for N_2, a major component in the gas phase.

$CO_2 + H_2 \rightleftharpoons CO + H_2O$ Equation 2

$CO + 3H_2 \rightleftharpoons CH_4 + H_2O$ Equation 3

$2CO + 2H_2 \rightleftharpoons CH_4 + CO_2$ Equation 4

$CO_2 + 4H_2 \rightleftharpoons CH_4 + 2H_2O$ Equation 5

Channel 18, related to H_2O, has also been plotted (cf. figure 3 (d)). No evident trend but a slight decrease with time could be observed. However, water was detected in the same order of magnitude as in the blank measurement: it therefore appears not certainly representative of real changes in the gaseous phase. However, water formation followed by its fast reaction with Na excess – resulting in low steady H_2O content – could not be excluded.

Besides, thermodynamic calculations made on the simple (N_2-H_2 system) showed that a significant part of the introduced nitrogen can react with dihydrogen to form ammonia, from approx. 3.6 bar at 300 °C to 2.7 bar at 380 °C, under 200 bar of total pressure [40]. Although conducted considering a simpler

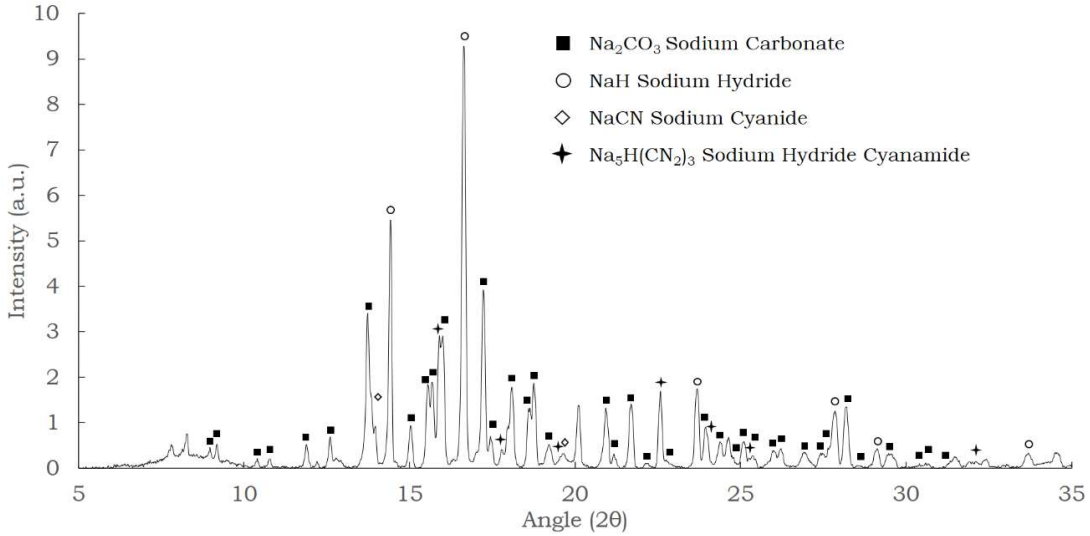

Figure 4: X-ray diffractogram of solvothermal product SP-T/350, indexed with sodium carbonate (PDF 37-0451), sodium hydride (PDF 76-0171), sodium cyanide (PDF 37-1490) and sodium hydride cyanamide (PDF 89-1367)

system than that in the solvothermal reactor, these calculations demonstrated the likely formation of ammonia during the process.

C.3. Solid phase characterization

C.3.1. X-Ray diffraction investigations

In order to further understand what species or bond could be formed during the solvothermal reaction, X-ray diffraction (XRD) has been carried out on sample SP-T/350 (same as SP-R/1.5). This sample being median in terms of solvothermal reaction temperature and Na/HEP ratio, every possible solid-state phases are expected to be present on its diffractogramshown in figure 4. The major part of diffraction peaks has been

indexed as sodium compounds such as sodium carbonate Na_2CO_3, sodium hydride NaH, sodium cyanide NaCN and sodium hydride cyanamide $Na_5H(CN_2)_3$. No peaks related to a crystalline carbon phase can be observed due to the lack of organization in the carbon-based network at this early stage of the synthesis.

XRD data allow to highlight what kind of environment is created during the solvothermal process. It is observed here that sodium does not only react with HEP but could also be involved in many secondary reactions. Sodium compounds are good indicators of the formation of the various molecules generated by HEP degradation. For instance, the presence of Na_2CO_3 likely reveals the formation of H_2O and CO_2, according to equations 6 to 8.

$$Na + H_2O \rightarrow (Na^+ OH^-) + ½H_2 \quad \text{Equation 6}$$
$$2OH^- + CO_2 \rightarrow CO_3^{2-} + H_2O \quad \text{Equation 7}$$
$$2Na^+ + CO_3^{2-} \rightarrow Na_2CO_3 \quad \text{Equation 8}$$

H_2 once formed, can also react with sodium to form sodium hydride revealed by XRD, according to equation 9 suggested formerly by Speyer et al. [15].

$$Na + ½H2 \rightarrow NaH \quad \text{Equation 9}$$

Sodium cyanide can be formed through different pathways. Each of them involves the earlier formation of simple molecules such as $NaNH_2$ or HCN, after equations 10 and 11 [41,42]:

$$NaNH_2 + C \rightarrow NaCN + H_2 \quad \text{Equation 10}$$
$$HCN + NaOH \rightarrow NaCN + H_2O \quad \text{Equation 11}$$

$NaNH_2$ can be formed by the reaction of sodium with ammonia [43], while HCN can be produced via the reaction of methane with ammonia, respectively according to the Degussa (equation 12) and Andrussow (equation 13) processes [44].

$$Na + NH_3 \rightarrow NaNH_2 + ½H_2 \quad \text{Equation 12}$$
$$CH_4 + NH_3 \rightarrow HCN + 3H_2 \quad \text{Equation 13}$$

The thermal decomposition during solvothermal reaction of sodium hydride cyanamide $Na_5H(CN_2)_3$, revealed by the XRD indexation, might lead to the formation of NaCN during the solvothermal process. In the literature, the decomposition of sodium cyanamide Na_2CN_2 has been shown to yield NaCN, Na and N_2 [45], according to equation 14.

$$Na_2CN_2 \rightarrow 2NaCN + Na + N_2 \quad \text{Equation 14}$$

It is suggested here that a similar reaction could occur during the solvothermal process starting from $Na_5H(CN_2)_3$. However, the formation of $Na_5H(CN_2)_3$ during the solvothermal reaction is not well understood yet.

C.3.2. Raman spectroscopy investigations

Raman spectroscopy has been used here to better characterize the solvothermal product in terms of density of π-conjugated bonds. For the sake of comparison, spectra of HEP and sample

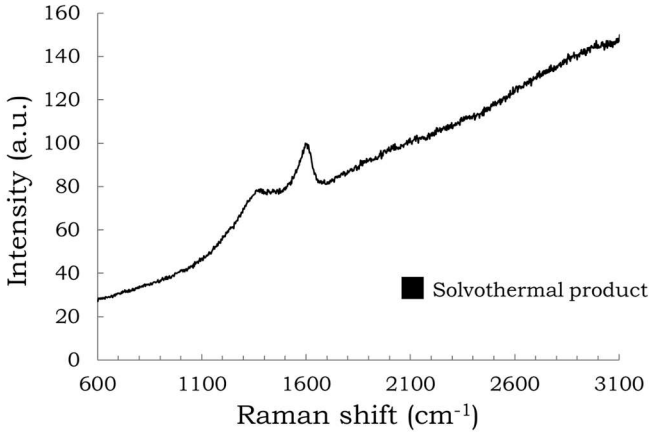

Figure 5: Raman spectrum of the solvothermal product

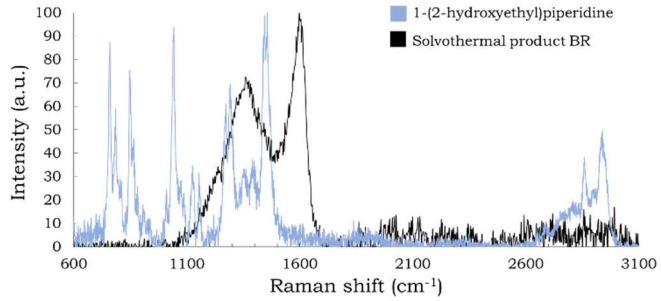

Figure 6: Raman spectra of HEP (blue) and solvothermal product BR (black)

SP-T/350 have been recorded in the range 600 cm^{-1} - 3100 cm^{-1} using a 532 nm wavelength laser (cf. figure 6 and 7).

Two interesting features in the form of two large bands appear on the solvothermal product spectrum at 1374 cm^{-1} and 1605 cm^{-1}, corresponding to the well-known carbon bands D and G respectively [46–48]. A high content of organized sp^2 carbon atoms is thus likely to be present after the solvothermal reaction as indicated by the G band, the intense and broad D band indicating the presence of numerous defects such as amorphous carbon, aliphatic fraction or defects in the graphenic network. Strong fluorescent background indicates the existence of high molecular weight aromatic molecules, with a high number of π-conjugated bonds. The more conjugated the π-system, the higher the Raman shift towards high wavelengths. For the sake of clarity, the fluorescent background has been removed using computational using computational tools, giving the spectrum referred as solvothermal product BR (standing for background removed).

The HEP spectrum in figure 7 shows many characteristic bands in the studied range, none of them being present in the solvothermal product BR spectrum. From this observation, the conversion of HEP during the solvothermal process appears total.

D Proposed overall mechanism

The first part of this work shows the broad source of information obtained on the solvothermal reaction between sodium and 1-(2-hydroxyethyl)piperidine using complementary analytical techniques. It has been first observed that after each solvothermal reaction, an overpressure and a loss of mass were noticed. It has been shown that a direct correlation between these two phenomena cannot explain the observations. Therefore, occurrence of several reactions has been suggested from the results of mass spectroscopy and XRD investigations, mainly linked to thermal degradation of HEP and EP-ONa into smaller molecules such as CO_2, H_2O or CH_4, as well as reactions between the excess of sodium and various species. Raman spectroscopy has revealed the early formation of sp^2 hybridized carbon atoms, in both graphitic domains and large aromatic molecules. The second part of this work aims to make bridges between these results to propose an overall mechanism of the solvothermal reaction.

D.1. Reaction pathway

D.1.1. First reactional stage

Based on the in-situ mass spectrometry observations, the expected reaction between HEP and Na (equation 1) is likely to start as soon as the reagents are put in contact. The stabilization of the channels related to H_2 and EP-ONa after a few hours indicated nearly terminated reaction. Moreover, the total conversion of HEP to EP-ONa has been confirmed by Raman spectroscopy as no traces of the initial reagent have been detected in the final product.

The large increase in H_2 concentration (related to equation 1) within the first hours goes along with a significant elevation of the CO_2, CH_4 and NH_3 levels. The formation of these products can be assigned to thermal degradation of EP-ONa, methanation reactions or reactions within the gaseous phase, e.g. ammonia formation from N_2 and H_2.

D.1.2. Second reactional stage

Throughout the whole solvothermal reaction, sodium can react with numerous molecules, e.g. H_2, H_2O, CH_4, NH_3, leading to the formation of numerous solid molecules such as NaH, Na_2CO_3, NaCN, NaOH or $NaNH_2$. These secondary reactions are of first importance as they allow the conversion of the liquid phase, supposedly formed from a mixture of H_2O, NH_3 and various C_xH_y molecules, and a part of the gaseous phase into a solid phase. As a matter of fact, it has been observed that for Na/HEP ratio equal to unity, the conversion of liquid products is far from complete, as shown by the very oily aspect of the product recovered. On the contrary for higher Na/HEP ratio, the fraction of liquid converted to a solid phase increases.

In the meanwhile, the solid phase, mainly composed of carbon, nitrogen and oxygen atoms, undergoes rearrangement reactions promoting the formation of large aromatic molecules, with a high number of π-conjugated bonds, as well as sp^2 carbon networks. Elimination reactions are likely to occur as they become predominant over substitution reactions at high temperature and under alkaline conditions [49]. Condensation reactions, aromatization reactions and cyclization reactions are likely to take place during the solvothermal process.

D.2. Description of the solvothermal products

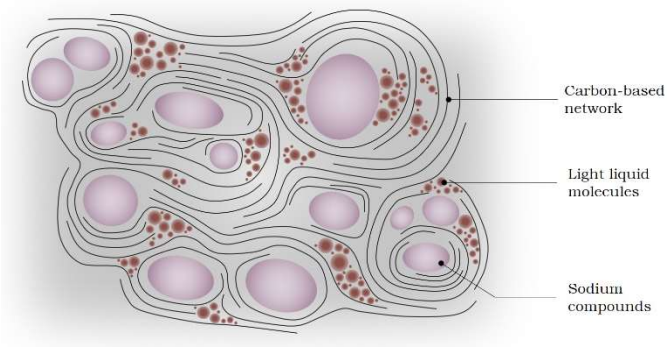

Figure 7: Drawing of the proposed structure for the solvothermal solid product before opening the reactor

At the end of the solvothermal reaction, before the opening of the reactor, the solid phase composed of a carbon-based network is likely to entrap solid sodium compounds as well as liquid or gaseous small molecules (cf. figure 8). The gaseous phase contains most of the initial N_2 injected before heating up the reactor, as well as H_2, NH_3, CO_2, CH_4 and probably other light C_xH_y molecules. The overall gases formed during the reaction are responsible for the increase in pressure, as reported in table 1.

When the reactor is opened, the sudden change in pressure, from around 75-85 bar to atmospheric pressure, is likely to cause the vaporization or sublimation of one part of the entrapped light molecules, which are ejected from the reactor. The presence of these molecules is not taken into account neither when measuring the pressure nor when measuring the mass amount. This phenomenon could explain the calculated yields below 70 wt.%.

Conclusions

The solvothermal reaction between metallic sodium and 1-(2-hydroxyethyl)piperidine yields a carbon-rich product, whose pyrolysis at 850 °C has been previously showed to lead to appealing 3-dimensional N-doped graphenic materials. In the present study, the impact of the solvothermal temperature and pressure, as well as the molar ratio between Na and HEP have been investigated. An increase in temperature, from 300 °C to 380 °C, has been shown to promote the conversion of the liquid phase into solid and gaseous compounds. It can be assumed that at high temperature, elimination reaction as well as other rearrangement reactions are more predominant than at lower temperatures. A rise in the Na/HEP ratio, from 1.0 to 2.0, has been revealed to contribute to various reactions between the excess of sodium and small molecules, e.g. CH_4, NH_3 or H_2O. Change in pressure, from 100 bar to 200 bar, has not been associated with meaningful variations in the solvothermal product. However, as it has been mentioned in a previous work [33], the pyrolysis of solvothermal products from 100-bar reactions lead only to poorly organized graphenic materials. This could mean that the solvothermal pressure has an impact on the structure and microstructure of the solvothermal product, but this could not be investigated since the synthetized products are unstable under electronic beam.

Complementary characterization techniques have been carried out to understand how the solvothermal reaction proceeds. In-situ mass spectrometry has shown the formation of H_2, CH_4, NH_3, and CO_2 throughout the synthesis, linked with the reaction between HEP and Na, methanation reactions as well as possible thermal degradation. The presence of these small molecules has been successfully related to XRD results, revealing the formation of various sodium compounds such as Na_2CO_3, NaH or NaCN. Raman spectroscopy has demonstrated the early formation of large sp^2 carbon network as well as molecules containing numerous π-conjugated bounds.

The various sources of data collected have led to an overall mechanism proposal which could hopefully help to better understand this type of reactions under strongly alkaline conditions, in a temperature and pressure domain still little known in organic synthesis. The schematic development still remains incomplete, in particular because of the complexity and the diversity of the phases present. Further work would require more thorough analysis of the oils and tars formed, as done for middle temperature range conversion of biomass for instance. Besides, the link between the solvothermal mixture and the highly structured products formed after pyrolysis is currently being investigated and will be thoroughly treated in a further paper. The first results tend to show that the pressure inside the reactor plays a role on the porous structure of the graphenic foams, low pressures being more favourable to the apparition of higher porosity, at the cost of a lower crystallinity. In the other hand, the reaction temperature seems linked with the chemical composition of the graphenic foams, as well as the crystallinity and the porosity. A break in trends tends to occur between the properties of the graphenic foams elaborated from the solvothermal reaction temperature of 350 °C and 380 °C. This observation could be a marker of the transition from a subcritical reaction to a supercritical reaction. Further investigations will be carried out to clarify this hypothesis.

Conflicts of interest

There are no conflicts to declare.

Acknowledgements

This work was supported partly by the French PIA project “Lorraine Université d’Excellence”, reference ANR-15-IDEX-04-LUE.

Notes and references

1 C. Aymonier, A. Loppinet-Serani, H. Reverón, Y. Garrabos and F. Cansell, *The Journal of Supercritical Fluids*, 2006, **38**, 242–251.
2 C. Erkey, in *Supercritical Fluid Science and Technology*, Elsevier, 2011, **1**, pp. 11–19.
3 N.-W. Pu, C.-A. Wang, Y. Sung, Y.-M. Liu and M.-D. Ger, *Materials Letters*, 2009, **63**, 1987–1989.
4 D. Rangappa, K. Sone, M. Wang, U. K. Gautam, D. Golberg, H. Itoh, M. Ichihara and I. Honma, *Chemistry - A European Journal*, 2010, **16**, 6488–6494.
5 L. Baldino, M. Sarno, S. Cardea, S. Irusta, P. Ciambelli, J. Santamaria and E. Reverchon, *Ind. Eng. Chem. Res.*, 2015, **54**, 8147–8156.
6 J. Yang, M. Wu, F. Chen, Z. Fei and M. Zhong, *The Journal of Supercritical Fluids*, 2011, **56**, 201–207.
7 X. Zhang, Z. Sui, B. Xu, S. Yue, Y. Luo, W. Zhan and B. Liu, *J. Mater. Chem.*, 2011, **21**, 6494.
8 X. Wu, J. Zhou, W. Xing, G. Wang, H. Cui, S. Zhuo, Q. Xue, Z. Yan and S. Z. Qiao, *J. Mater. Chem.*, 2012, **22**, 23186.
9 K. Mase, H. Kondo, S. Kondo, M. Hori, M. Hiramatsu and H. Kano, *Appl. Phys. Lett.*, 2011, **98**, 193108.
10 S. P. Sasikala, P. Poulin and C. Aymonier, *Adv. Mater.*, 2017, **29**, 1605473.
11 Kuang, S.-Y. Xie, Z.-Y. Jiang, X.-H. Zhang, Z.-X. Xie, R.-B. Huang and L.-S. Zheng, *Carbon*, 2004, **42**, 1737–1741.
12 Eftekhari and P. Jafarkhani, *J. Phys. Chem. C*, 2013, **117**, 25845–25851.

13 M. Choucair, P. Thordarson and J. A. Stride, *Nature Nanotech*, 2009, **4**, 30–33.
14 L. Speyer, S. Fontana, S. Cahen, J. Ghanbaja, G. Medjahdi and C. Hérold, *Solid State Sciences*, 2015, **50**, 42–51.
15 L. Speyer, S. Fontana, S. Ploneis and C. Hérold, *Microporous and Mesoporous Materials*, 2017, **243**, 254–262.
16 L. Speyer, S. Fontana, S. Cahen and C. Hérold, *Materials Chemistry and Physics*, 2018, **219**, 57–66.
17 H. Cui, J. Zheng, P. Yang, Y. Zhu, Z. Wang and Z. Zhu, *ACS Appl. Mater. Interfaces*, 2015, **7**, 11230–11238.
18 P. Yan, J. Liu, S. Yuan, Y. Liu, W. Cen and Y. Chen, *Applied Surface Science*, 2018, **445**, 398–403.
19 J. Huang, J. Han, T. Gao, X. Zhang, J. Li, Z. Li, P. Xu and B. Song, *Carbon*, 2017, **124**, 34–41.
20 M. Li, Z. Liu, F. Wang and J. Xuan, *Journal of Energy Chemistry*, 2017, **26**, 422–427.
21 H. L. Tan, A. Du, R. Amal and Y. H. Ng, *Chemical Engineering Science*, 2019, **194**, 85–93.
22 J. Guo, S. Gadipelli, Y. Yang, Z. Li, Y. Lu, F. J. L. Brett and Z. Guo, *J. Mater. Chem. A*, 2019, **7**, 3544-3551
23 L. S. Panchakarla, K. S. Subrahmanyam, S. K. Saha, A. Govindaraj, H. R. Krishnamurthy, U. V. Waghmare and C. N. R. Rao, *Adv. Mater*., 2009, **21**, 4726-4730.
24 Z. Wang, P. Li, Y. Chen, J. Liu, H. Tian, J. Zhou, W. Zhang and Y. Li, *J. Mater. Chem*. C, 2014, **2**, 7396.
25 D. Li, X. Duan, H. Sun, J. Kang, H. Zhang, M. O. Tade and S. Wang, *Carbon*, 2017, **115**, 649–658.
26 C. S. Ramirez-Barria, D. M. Fernandes, C. Freire, E. Villaro-Abalos, A. Guerrero-Ruiz and I. Rodriguez-Ramos, *Nanomaterials*, 2019, **9**, 1761
27 Z. Xing, X. Luo, Y. Qi, W. F. Stickle, K. Amine, J. Lu and X. Ji, *ChemNanoMat*, 2016, **2**, 692-697
28 J. Moon, J. An, U. Sim, S.-P. Cho, J. H. Kang, C. Chung, J.-H. Seo, J. Lee, K. T. Nam and B. H. Hong, *Adv. Mater*., 2014, **26**, 3501–3505.
29 X. Chen, D. Deng, X. Pan, Y. Hu and X. Bao, *Chem. Commun*., 2015, **51**, 217–220.
30 D. Deng, X. Pan, L. Yu, Y. Cui, Y. Jiang, J. Qi, W.-X. Li, Q. Fu, X. Ma, Q. Xue, G. Sun and X. Bao, *Chem. Mater*., 2011, **23**, 1188–1193.
31 R. Ma, X. Ren, B. Y. Xia, Y. Zhou, C. Sun, Q. Liu, J. Liu and J. Wang, *Nano Res*., 2016, **9**, 808–819.
32 S. M. Lyth, Y. Nabae, N. Md. Islam, T. Hayakawa, S. Kuroki, M. Kakimoto and S. Miyata, *e-J. Surf. Sci. Nanotech*., 2012, **10**, 29–32.
33 L. Moumaneix, S. Fontana, M. Dossot, F. Lapicque and C. Hérold, *Microporous and Mesoporous Materials*, 2020, DOI: 10.1016/j.micromeso.2020.110165.
34 C. H. Tu, Chemical Engineering Science, 1995, 50, 3515–3520.
35 J. Marrero and R. Gani, *Fluid Phase Equilibria*, 2001, **183–184**, 183–208.
36 J. Li, L. Xia and S. Xiang, *Fluid Phase Equilibria*, 2016, **417**, 1–6.
37 G. Demazeau, *J. Phys.: Conf. Ser*., 2010, **215**.
38 S. Rönsch, J. Schneider, S. Matthischke, M. Schlüter, M. Götz, J. Lefebvre, P. Prabhakaran and S. Bajohr, *Fuel*, 2016, **166**, 276–296.
39 K. Ghaib, K. Nitz and F.-Z. Ben-Fares, *ChemBioEng Reviews*, 2016, **3**, 266–275.
40 V. Kaiser, E. Filippi, H. D. Léger and P. Lesur, *Techniques de l'ingénieur*, 1999, **J4 040**, 1-16 [in French].
41 A. Rubo, R. Kellens, J. Reddy, N. Steier and W. Hasenpusch, in *Ullmann's Encyclopedia of Industrial Chemistry*, ed. Wiley-VCH Verlag GmbH & Co. KGaA, Weinheim, Germany, 2006, DOI: 10.1002/14356007.i01_i01.
42 M. F. Ray & M. Rajchel, US 6 649 136 B2, 2003.
43 K. W. Greenlee, A. L. Henne and W. C. Fernelius, in *Inorganic Syntheses*, ed. W. C. Fernelius, John Wiley & Sons, Inc., Hoboken, NJ, USA, 2007, 128–135.
44 E. Formentin & C. Schafer, EP 2 260 002 B1, 2011.
45 M. J. Sole and A. D. Yoffe, *Proc. R. Soc. Lond. A*, 1964, **277**, 523–539.
46 K. Sasaki, Y. Tokura and T. Sogawa, *Crystals*, 2013, **3**, 120–140.
47 R. J. Nemanich and S. A. Solin, *Phys. Rev. B*, 1979, **20**, 392–401.
48 M. S. Dresselhaus, A. Jorio and R. Saito, *Annu. Rev. Condens. Matter Phys*., 2010, **1**, 89–108.
49 L. P. Wolters, Y. Ren and F. M. Bickelhaupt, *ChemistryOpen*, 2014, **3**, 29–36.